JOURNAL OF Materials CHEMISTRY

Sol–gel deposition and luminescent properties of oxyapatite $Ca_2(Y,Gd)_8(SiO_4)_6O_2$ phosphor films doped with rare earth and lead ions

M. Yu, J. Lin,* Y. H. Zhou, S. B. Wang and H. J. Zhang

Key Laboratory of Rare Earth Chemistry and Physics. Changchun Institute of Applied Chemistry, Chinese Academy of Sciences, Changchun 130022, P. R. China. E-mail: jlin@ns.ciac.jl.cn

Received 27th June 2001, Accepted 8th October 2001
First published as an Advance Article on the web 26th November 2001

Rare-earth and lead ions (Eu^{3+}, Tb^{3+}, Dy^{3+}, Pb^{2+}) doped $Ca_2Y_8(SiO_4)_6O_2$ and $Ca_2Gd_8(SiO_4)_6O_2$ thin films have been dip-coated on silicon and quartz glass substrates through the sol–gel route. X-Ray diffraction (XRD), TG–DTA, scanning electron microscopy (SEM), atomic force microscopy (AFM), FT-IR and luminescence excitation and emission spectra as well as luminescence decays were used to characterize the resulting films. The results of XRD reveal that these films remain amorphous below 700 °C, begin to crystallize at 800 °C and crystallize completely around 1000 °C with an oxyapatite structure. The grain structure of the film can be seen clearly from SEM and AFM micrographs, where particles with various shapes and average size of 250 nm can be resolved. Eu^{3+} and Tb^{3+} show their characteristic red ($^5D_0$–$^7F_2$) and green ($^5D_4$–$^7F_5$) emission in the films with a quenching concentration of 10 and 6 mol% (of Y^{3+}), respectively. The lifetime and emission intensity of Eu^{3+} increase with the temperature treatment from 700 to 1100 °C, while those of Tb^{3+} show a maximum at 800 °C. Energy transfer phenomena have been observed by activating the oxyapatite film host-lattice $Ca_2Gd_8(SiO_4)_6O_2$ with Tb^{3+} (Dy^{3+}). In addition, Pb^{2+} can sensitize the Gd^{3+} sublattice in $Ca_2Gd_8(SiO_4)_6O_2$.

Luminescent thin films have been attracting much attention for their potential application in high-resolution devices such as cathode ray tubes (CRTs), flat panel display devices and field emission displays (FEDs).[1–3] Compared with conventional display screens prepared by deposition of fine grain luminescent powders, displays with thin film phosphors have higher contrast, superior thermal conductivity as well as a high degree of uniformity and better adhesion.[4] In addition, the uniform thickness combined with smoother surface morphology and smaller grain size make it possible to obtain smaller pixel spot sizes to achieve a higher resolution.[5] Efforts have been made in the past decade to develop various types of luminescent films *via* the sol–gel method. Representative examples are $Y_2SiO_5:Tb$[6] and $Y_3Al_5O_{12}:Tb$[7] films for cathodoluminescence, $Y_3Al_5O_{12}:Eu$[8] and $Y_3(Al, Ga)_5O_{12}:Tb$[9] films for field emission displays, $Y_2O_3:Eu$,[10] $TiO_2:Eu$[11] and $Zn_2SiO_4:Mn/Tb$[12,13] films for photoluminescence, and $ZnS:Mn/Tb$[14] and $Ga_2O_3:Eu/Mn$[15] films for electroluminescence. However, so far the total number of publications in this field has not been over twenty. Recently we have published a review concerning the progress of luminescent films fabricated *via* the sol–gel method.[16]

$Ca_2RE_8(SiO_4)_6O_2$ (RE = Y or Gd) are ternary rare-earth-metal silicates with oxyapatite structure, which have been used as host materials for the luminescence of various rare earth and mercury-like ions.[17–20] The most prominent structural characteristic is the two rare-earth sites in the oxyapatite host lattice, *i.e.*, the nine-coordinate 4f site with C_3 point symmetry and the seven-coordinate 6h site with C_s point symmetry. Both sites are very suitable for the luminescence of rare earth ions due to their low symmetry features.[17–20] So far no report has been published on luminescent films based on these materials. In order to emphasize the significance of luminescent films prepared by the sol–gel method, we report the structural and luminescent properties of rare earth (Eu^{3+}, Tb^{3+}) and lead ions (Pb^{2+})-doped oxyapatite $Ca_2RE_8(SiO_4)_6O_2$ (RE = Y or Gd) films deposited by this method.

Experimental

The starting materials used for preparation of the phosphor films were $CaCO_3$ (A.R), Y_2O_3 (99.99%), Eu_2O_3 (99.99%), Tb_4O_7 (99.99%), Dy_2O_3 (99.99%), $Pb(NO_3)_2$ (A.R), Gd_2O_3 (99.99%) and tetraethoxysilane $Si(OC_2H_5)_4$ (TEOS). The preparation of the samples consists of three steps: synthesis of the coating solution, film deposition, and subsequent heat treatment.

Synthesis of the coating solutions

The preparation of the coating solutions is as follows. First, stoichiometric amounts of the starting materials were dissolved in dilute HNO_3; second, a suitable amount of ethanol was added to this solution under stirring until a homogeneous phase formed; third, a stoichiometric amount of TEOS dissolved in ethanol was added to the above solution with magnetic stirring at room temperature, and the pH value of this solution was kept between one and three. The obtained sol which was highly transparent and remained stable for several weeks if sealed, was then ready for film deposition.

Film deposition

The substrates (quartz glasses and silicon wafers) were pre-cleaned in a 5 wt% KOH ethanol solution for fifteen minutes, followed by a five-minute dipping in 1 M HCl to neutralize the alkali attack on the glass surface, and then soaked in pure water for twenty minutes. Finally they were thoroughly ultrasonicated in ethanol for twenty minutes. The cleaned substrates were then dipped into the coating solution before being slowly withdrawn from the solution with a speed of 0.5 cm s^{-1}. Samples were then baked at 120 °C for 5 h immediately after coating. The dried films were then annealed to 500 °C for 2 h in a furnace with a heating rate of 60 °C h^{-1}. The preheated film

 DOI: 10.1039/b105644c

samples were then fired at a rate of 100 °C h^{-1} to the desired temperature (700–1100 °C) and held at this temperature for 2 h.

Characterization

X-Ray diffraction (XRD) patterns of the film samples were recorded on a Rigaku-Dmax 2500 diffractometer using Cu Kα radiation ($\lambda = 0.15405$ nm). FT-IR spectra were measured on a Perkin-Elmer 580B infrared spectrophotometer using the KBr pellet technique. A DT-30 Shimadzu thermal analyzer was used for recording TGA–DTA curves of the gel powders. The morphology of crystalline film samples were inspected using a scanning electron microscope (JEOL JXA-840) and an atomic force microscope (AFM, Seiko) in tapping mode. Excitation and emission spectra were obtained on a SPEX FL-2T2 spectrofluorometer equipped with a 450 W xenon lamp as the excitation source. Luminescence lifetimes were measured with a SPEX 1934D phosphorimeter using a 7 W pulse xenon lamp as the excitation source with a pulse width of 3 μs. All measurements were performed at room temperature (RT).

Results and discussion

Formation process and morphology of the phosphor films

XRD. Fig. 1 shows XRD patterns of film samples annealed at different temperatures from 700 to 1100 °C at intervals of 100 °C. For films annealed below 700 °C, no diffraction peaks are observed except for a broad band at $2\theta = 22°$, ascribed to quartz glass substrate. This indicates that the film remains amorphous below this temperature. For the sample fired at 800 °C, a weak and broad peak at $2\theta = 29.8°$ is present in the XRD pattern, which is assigned to (210) reflection of oxyapatite $Ca_2Y_8(SiO_4)_6O_2$, suggesting the starting of crystallization at this stage. At 900 °C, other diffraction peaks at $2\theta = 22.6°$ (200), 23.7° (111), 26.9° (002), 29.1° (102), 32.7° (211) 33.3° (112) and 33.8° (300) belonging to crystalline oxyapatite are observed (JCPDS Card 27-93). These diffraction peaks increase in intensity with further increase of the annealing temperature, and no difference in width and intensity is observed for the 1000 °C and 1100 °C sintered samples, indicating that the crystallization of $Ca_2Y_8(SiO_4)_6O_2$ is complete at 1000 °C. This temperature is about 300 °C lower than that of the powder $Ca_2Y_8(SiO_4)_6O_2$ sample prepared by solid state reaction of carbonate and oxides, thus illustrating the advantage of the sol–gel method.[21]

TG–DTA. The thermogravimetric and differential thermal analysis (TG–DTA) curves of the gel sample dried at 70 °C are shown in Fig. 2. The gel sample shows rapid weight loss around 140 °C, with endothermic peaks at 119 and 152 °C, which result from the evaporation of residual water and ethanol in the powder gel. The endothermic peaks at 325 and 455 °C correspond to the decomposition of the organic compounds and nitrates in the gel. No weight loss occurs beyond 500 °C. The exothermic peak at 915 °C is due to the crystallization of the gel, agreeing well with the results of XRD analysis.

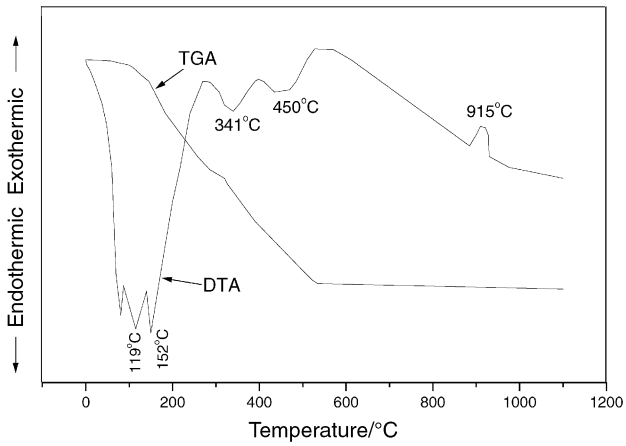

Fig. 2 TGA–DTA curves of the dry gel powder obtained from the coating sol.

FT-IR spectra. FT-IR spectra were recorded for the films on silicon wafers at various stages of heat treatment, as shown in Fig. 3. For the gel film after heat treatment at 120 °C, the IR spectrum shows three main regions of interest: the first (a broad band) in the range 2750–3750 cm^{-1} with a maximum at 3488 cm^{-1}, arises from the absorption of O–H groups; the second region in the range 1250–1750 cm^{-1}, which originates from the absorption of H_2O (1640 cm^{-1}) and NO_3^- groups (1480, 1320 cm^{-1}); and the third region with peaks at 1000–1170 cm^{-1}, which are assigned to the absorption of Si–O–Si asymmetric stretching vibrations. Significant changes are observed with further heat treatment. After heating at 500 °C, the absorption peaks from –OH, H_2O and NO_3^- almost disappear, and a new broad absorption band peaking at 950 cm^{-1} is present, which arises from the asymmetric stretching vibration of SiO_4 groups. After heat treatment at 700 °C, the absorption of H_2O and NO_3^- disappear completely, indicating the complete evaporation of H_2O and the pyrolysis of nitrate; meanwhile, a new absorption peak at 553 cm^{-1} due to bending vibration of O–Si–O bonds is present,

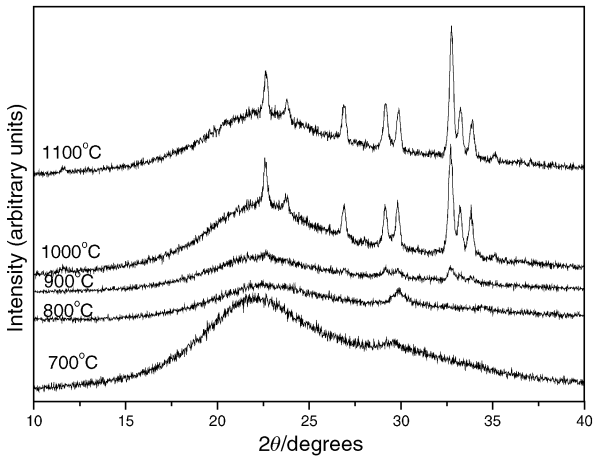

Fig. 1 XRD patterns of $Ca_2Y_{7.2}Eu_{0.8}(SiO_4)_6O_2$ films on quartz glass after heat treatment at different temperatures.

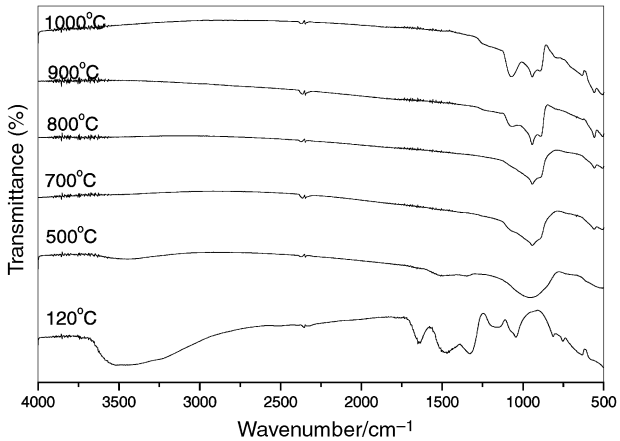

Fig. 3 FT-IR spectra of $Ca_2Y_{7.2}Eu_{0.8}(SiO_4)_6O_2$ films on silicon wafers as a function of annealing temperature.

and the absorption bands of SiO_4 groups remain broad implying the amorphous character of the film. Heat treatment between 800 to 1000 °C leads the absorption peaks of SiO_4 to be more structured, suggesting that crystallized silicate oxyapatite has formed in the film. Note that the broad absorption peak at 1076 cm^{-1} becomes stronger with increasing the heat treatment temperature after 900 °C. In fact, in the IR spectrum of pure silicon wafer without any film, this peak also exists and its intensity increases with raising the treatment temperature. Therefore, this peak can be attributed to the absorption of Si–O–Si bonds in SiO_2, which formed on the surface of the silicon wafer due to the oxidation of silicon at high temperatures.

Morphology of the films. The morphology of a $Ca_2Y_8(SiO_4)_6O_2$: Eu film deposited on quartz glass was investigated by SEM and AFM. The grain structure of the film can be seen clearly from SEM and AFM. The SEM images of the surface and cross-section of an opaque $Ca_2Y_8(SiO_4)_6O_2$: Eu film sintered at 1000 °C are shown in Fig. 4(a) and (b), respectively. From the surface image of the film we can observe that the film consists of fine closely packed particles with an average size of 250 nm (Fig. 4(a)). From the SEM image for the cross-section of the film (Fig. 4(b)) it is evident that the film is uniform in thickness, *ca.* 2.66 μm. The surface morphology can be observed more clearly by AFM as shown in Fig. 5, where different shapes (triangular, spherical *etc.*) of particles can be resolved.

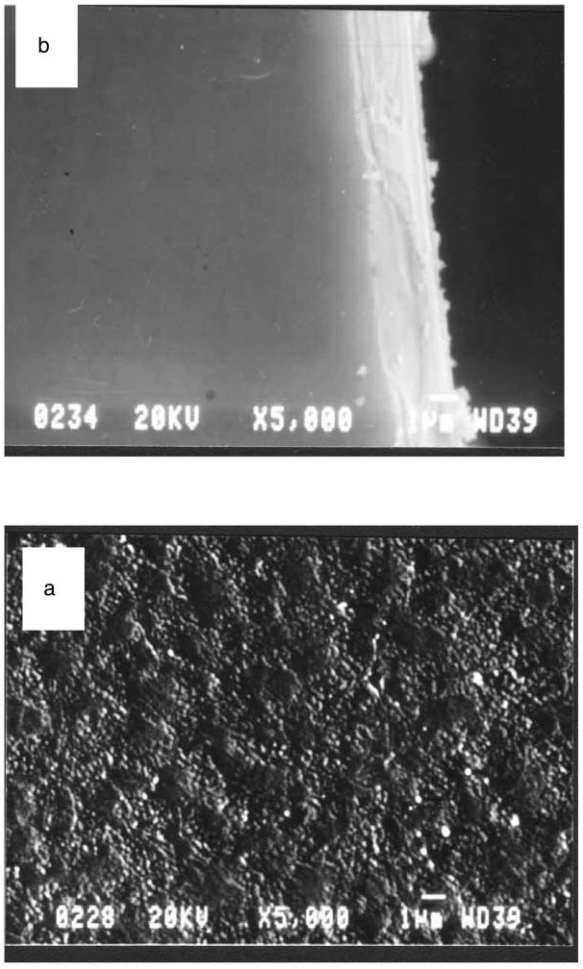

Fig. 4 SEM images of the surface (a) and cross-section (b) of a $Ca_2Y_{7.2}Eu_{0.8}(SiO_4)_6O_2$ film sintered at 1000 °C.

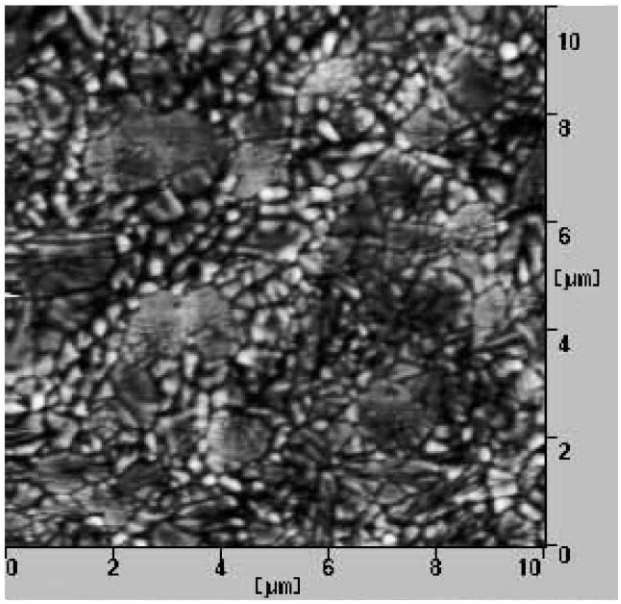

Fig. 5 AFM image of $Ca_2Y_{7.2}Eu_{0.8}(SiO_4)_6O_2$ film sintered at 1000 °C.

Photoluminescence properties. The photoluminescence properties of the films were studied by excitation and emission spectra as well as luminescence decays.

$Ca_2Y_8(SiO_4)_6O_2$: Eu^{3+} films. Fig. 6 shows the excitation and emission spectra for $Ca_2Y_{7.2}Eu_{0.8}(SiO_4)_6O_2$ films. The excitation spectrum (Fig. 6(a)) consists of a broad intense band with a maximum at 269 nm and some weak lines. The former is due to the charge transfer band (CTB) of Eu^{3+}–O^{2-}, and the latter are from the f–f transitions within the Eu^{3+} $4f^6$ electron configuration. The emission spectra were recorded as a function of annealing temperature (Fig. 6(b)). Upon excitation

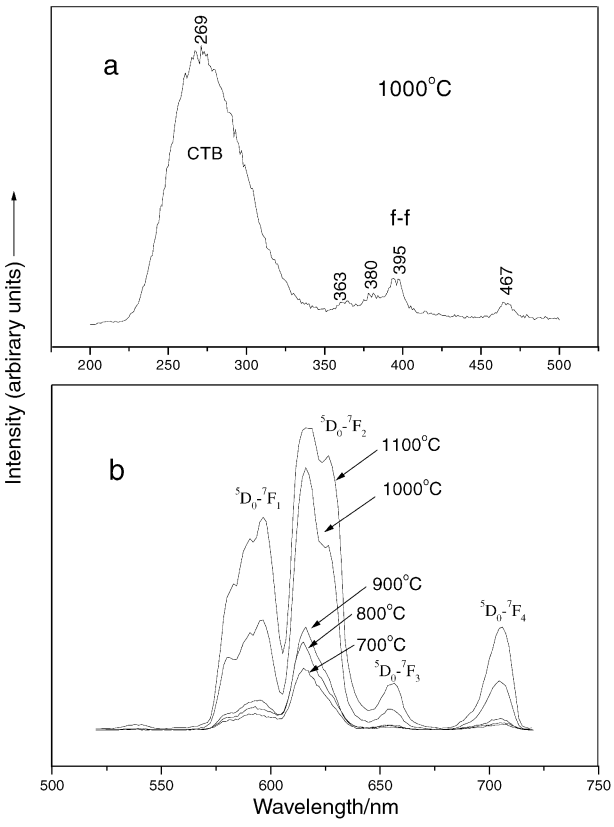

Fig. 6 Excitation (a) and emission (b) spectra of $Ca_2Y_{7.2}Eu_{0.8}(SiO_4)_6O_2$ films (annealed at various temperatures for emission).

into the CTB at 269 nm, all the emission spectra are composed of $^5D_0$–^7F_J (J = 1, 2, 3, 4) emission lines of Eu^{3+}, with the hypersensitive red emission transition $^5D_0$–$^7F_2$ (616 nm) being the most prominent group, agreeing well with the low local symmetry (C_3 and/or C_s) for Eu^{3+} in the host lattice. Influenced by the background of the films, *i.e.* non-crystalline silica glass substrate, the spectral bands of Eu^{3+} seem to be broader than those in the crystalline powders, and the $^5D_0$–$^7F_0$ transition line of Eu^{3+} is hidden by the broad $^5D_0$–$^7F_1$ transition band.[17] In addition, no emission from higher ^5D_J ($J > 0$) levels is observed. This can be ascribed to the fact that the energy gaps between $^5D_2$ and $^5D_1$ and between $^5D_1$ and $^5D_0$ of Eu^{3+} are 2500 and 1750 cm^{-1} respectively, and so silicate groups with a maximum vibration energy of 950 cm^{-1} (evidenced by FT-IR spectra in Fig. 3) are able to bridge the gaps between the higher lying levels of the Eu^{3+} and the $^5D_0$ level.[17] With the increase of annealing temperature, the Eu^{3+} emission intensity increases and more spectral lines can be resolved. This is in accord with the fact that the crystallinity of the film increases with firing temperature, as shown in the XRD patterns (Fig. 1).

Photoluminescence decay curves of Eu^{3+} in $Ca_2Y_{7.2}Eu_{0.8}(SiO_4)_6O_2$ films sintered at various temperatures are shown in Fig. 7. In general, all these curves can be well fitted to a single exponential function as $I = I_0 + A\exp[-(t - t_0)/\tau]$ (A is constant, τ is the lifetime), from which the lifetimes of Eu^{3+} are determined and shown in Fig. 7. It is found that the lifetime of Eu^{3+} increases with the annealing temperature. This is due to the fact that the content of impurities in the film such as –OH, –OR, H_2O, NO_3^- *etc.* decreases with increase of annealing temperature. The quenching of the luminescence of Eu^{3+} by excitation of the vibrations of these impurities decreases, resulting in the increase of the lifetimes of Eu^{3+}. In addition, the lifetimes of Eu^{3+} have also been studied as a function of Eu^{3+} doping concentration in the films, as shown in Fig. 8. The lifetimes of Eu^{3+} first increase with dopant concentration, reaching a maximum at 10 mol%, and then decrease with further increasing the dopant concentration. This indicates concentration quenching of the luminescence of Eu^{3+} in the film host. The optimum concentration of Eu^{3+} is 10 mol% that of Y^{3+} in the $Ca_2Y_8(SiO_4)_6O_2$ host film.

$Ca_2Y_8(SiO_4)_6O_2:Tb^{3+}$ films. Fig. 9 shows the excitation and emission spectra of a $Ca_2Y_{7.84}Tb_{0.16}(SiO_4)_6O_2$ thin film. The excitation spectrum (Fig. 9(a)) of Tb^{3+} contains an intense broad band with a maximum at 246 nm with a shoulder at 277 nm and some weak excitation lines in the longer wavelength region within the Tb^{3+} $4f^8$ electron configuration. The strong excitation band at 246 nm is due to the spin-allowed

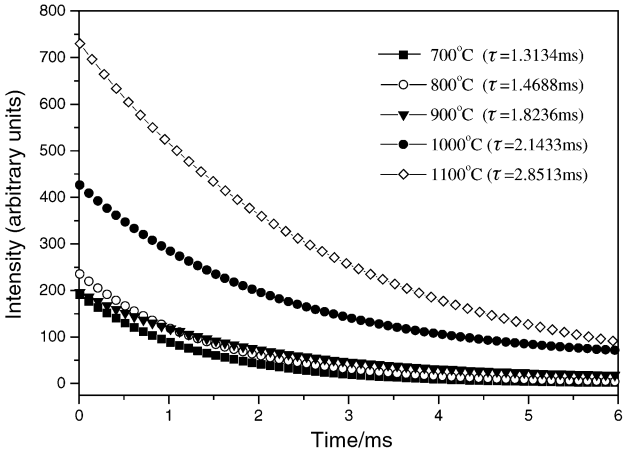

Fig. 7 Decay curves of Eu^{3+} luminescence in $Ca_2Y_{7.2}Eu_{0.8}(SiO_4)_6O_2$ thin films annealed at different temperatures. The values of lifetimes are indicated.

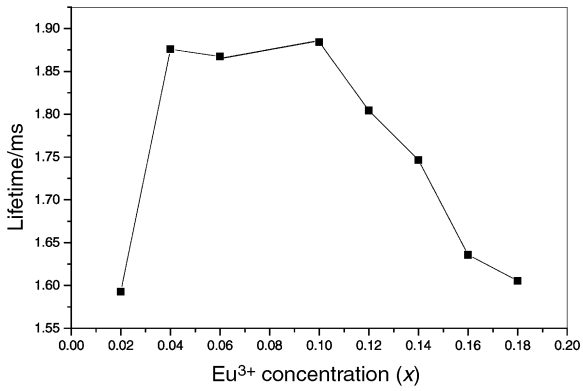

Fig. 8 Lifetimes of Eu^{3+} luminescence as a function of its doping concentration (x) in $Ca_2Y_{8(1-x)}Eu_{8x}(SiO_4)_6O_2$ films.

$4f^8$–$4f^7$5d transition ($\Delta S = 0$) and the shoulder is from the spin-forbidden component of $4f^8$–$4f^7$5d transition ($\Delta S = 1$), respectively.[18] Excitation into the spin-allowed $4f^8$–$4f^7$5d band at 246 nm yields the characteristic blue and green emission lines of Tb^{3+} $^5D_{3,4}$–^7F_J (J = 3, 4, 5, 6) transitions, with the $^5D_4$–$^7F_5$ (545 nm) green emission as the most prominent feature (Fig. 9(b)). Due to the cross-relaxation betwwen $^5D_3$–$^5D_4$ and $^7F_0$–$^7F_6$, the blue emission of $^5D_3$–^7F_J transition is weak.

Fig. 10 shows the dependence of the intensity of Tb^{3+} $^5D_4$–$^7F_5$ green emission and the lifetimes of the Tb^{3+} $^5D_4$ excited state on its concentration (x) in $Ca_2Y_{8(1-x)}Tb_{8x}(SiO_4)_6O_2$ films. Both the emission intensity and lifetimes of Tb^{3+} first increase with its doping concentration, reaching a maximum at x = 6 mol%, and then decrease with increasing Tb^{3+} concentration due to concentration quenching. Thus the optimum concentration for the Tb^{3+} green emission is 6 mol% that of Y^{3+} in $Ca_2Y_8(SiO_4)_6O_2$ films.

Furthermore, the lifetimes ($^5D_4$) and emission intensity of Tb^{3+}($^5D_4$–$^7F_5$) have also been studied as a function of the

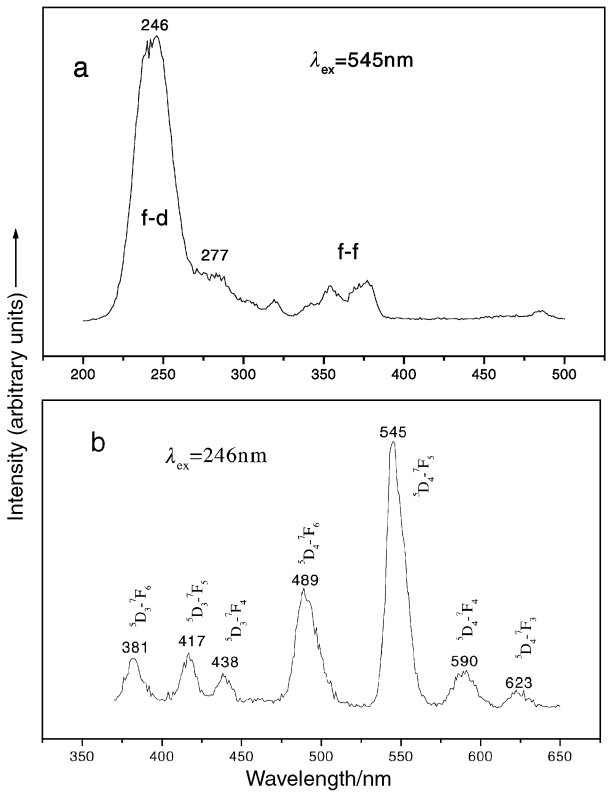

Fig. 9 Excitation (a) and emission (b) spectra of a $Ca_2Y_{7.84}Tb_{0.16}(SiO_4)_6O_2$ film.

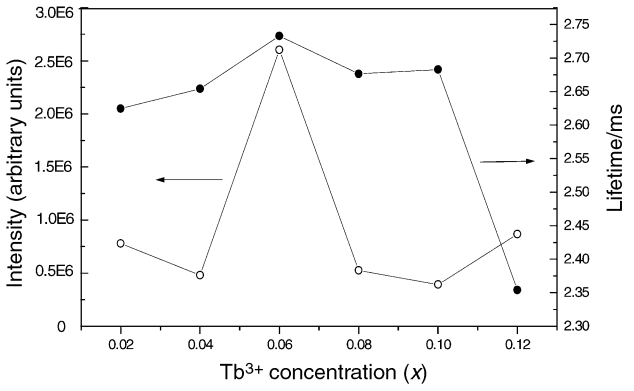

Fig. 10 Dependence of the relative emission intensity and lifetimes of Tb^{3+} luminescence on its doping concentration (x) in $Ca_2Y_{8(1-x)}Tb_{8x}(SiO_4)_6O_2$ films.

annealing temperature for the $Ca_2Y_{7.84}Tb_{0.16}(SiO_4)_6O_2$ film, as shown in Fig. 11. Differently from the results obtained with Eu^{3+} (the lifetime and emission intensity increase with an increase of the annealing temperature), both the Tb^{3+} lifetimes and emission intensity first increase sharply from 700 to 800 °C and then decrease sharply above 900 °C. This is because the Tb^{3+} is easily oxidized to Tb^{4+} at high temperature, with the latter acting as a quenching center for the luminescence of Tb^{3+}.

$Ca_2Gd_8(SiO_4)_6O_2:Pb^{2+}$, Tb^{3+} (Dy^{3+}) films. For comparison purposes, we also prepared Tb^{3+} and Pb^{2+}-codoped $Ca_2Gd_8(SiO_4)_6O_2$ films on quartz glass substrates. Under 254 nm excitation, the film shows bright green emission. Fig. 12 shows the excitation and emission spectra of Tb^{3+} and Pb^{2+}-codoped $Ca_2Gd_8(SiO_4)_6O_2$ and $Ca_2Y_8(SiO_4)_6O_2$ thin films. The excitation spectrum of Tb^{3+}- and Pb^{2+}-codoped $Ca_2Gd_8(SiO_4)_6O_2$ film consists of a strong absorption band with a maximum at 261 nm, which corresponds to the Pb^{2+} $^1S_0$–$^3P_1$ transition, followed by Gd^{3+} ^8S–^6I and ^8S–^6P transitions peaking at 277 and 313 nm, respectively. The presence of both Pb^{2+} and Gd^{3+} excitation indicates that energy transfer processes Pb^{2+}–Tb^{3+} and Gd^{3+}–Tb^{3+} occur in this film. Upon excitation into Pb^{2+} at 254 nm, the emission spectrum consists of a very weak Pb^{2+} emission band (background in the blue region) and a strong emission of Tb^{3+} with a maximum at 545 nm. However, energy transfer from Pb^{2+} to Tb^{3+} is far from complete at identical Pb^{2+} and Tb^{3+} concentrations for the $Ca_2Y_8(SiO_4)_6O_2$ film. The emission intensity of Tb^{3+} in $Ca_2Gd_8(SiO_4)_6O_2$ film is more than twice as strong as that in $Ca_2Y_8(SiO_4)_6O_2$ under excitation into Pb^{2+} at 254 nm. Thus the role of Gd^{3+} as an intermediate in the energy transfer

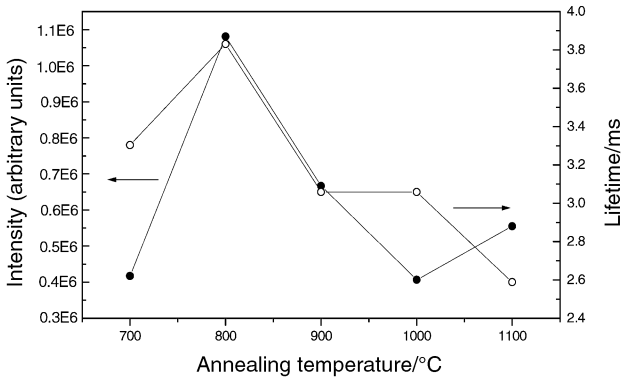

Fig. 11 Lifetimes and emission intensity of Tb^{3+} luminescence in $Ca_2Y_{7.84}Tb_{0.16}(SiO_4)_6O_2$ thin films as a function of annealing temperatures.

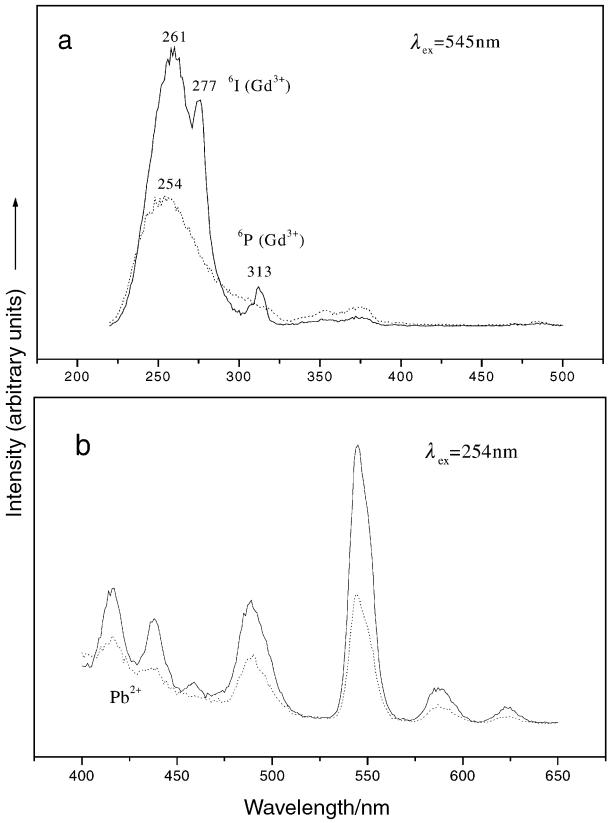

Fig. 12 Excitation (a) and emission (b) spectra of $Ca_{1.96}Pb_{0.04}RE_{7.9}Tb_{0.1}(SiO_4)_6O_2$ (RE = Gd; Y) thin films: (—) RE = Gd; (– – –) RE = Y.

process from Pb^{2+} to Tb^{3+} is clearly seen, *i.e.*, an energy migration process Pb^{2+}–Gd^{3+}–$(Gd^{3+})_n$–Tb^{3+} occurs in the $Ca_2Gd_8(SiO_4)_6O_2$ film. Dy^{3+} and Pb^{2+}-codoped $Ca_2Gd_8(SiO_4)_6O_2$ and $Ca_2Y_8(SiO_4)_6O_2$ thin films were also prepared on quartz glass, and showed similar behavior as above. These results for the film samples are similar to those obtained for powder samples of Pb^{2+} and Mn^{2+}-codoped $Sr_2Gd_8(SiO_4)_6O_2$.[22]

Conclusions

Luminescent thin films $Ca_2Y_8(SiO_4)_6O_2$ and $Ca_2Gd_8(SiO_4)_6O_2$ doped with rare earth and Pb^{2+} ions can be successfully deposited on quartz glass and silicon wafers by the sol–gel dip coating method. The films are uniform and crack free. They contain grains with an average size of 250 nm. From 700 to 1100 °C, the lifetimes and emission intensity of Eu^{3+} increase with the annealing temperature, while those of the Tb^{3+} show a maximum at 800 °C. The optimum concentrations of Eu^{3+} and Tb^{3+} in $Ca_2Y_8(SiO_4)_6O_2$ films are 10 and 6 mol% of Y^{3+}, respectively. The Pb^{2+} can sensitize the Gd^{3+}-sublattice in $Ca_2Gd_8(SiO_4)_6O_2$ films and enhance greatly the emission intensity of the codoped rare earth ions (Tb^{3+}, Dy^{3+}).

Acknowledgements

This project is financially supported by the foundation of "Bairen Jihua"of Chinese Academy of Sciences, the Outstanding Youth Fund of Jilin Province, and Personnel Ministry as well as Educational Ministry of China.

References

1 X. Ouyang, A. H. Kitai and T. Xiao, *J. Appl. Phys.*, 1997, **71**, 404.
2 G. A. Hirata, J. Mckittrick, M. Avalos-Borja, J. M. Siquetros and D. Devlin, *Appl. Surf. Sci.*, 1997, **113/114**, 509.

3 S. L. Jones, D. Kumar, R. K. Singh and P. H. Holloway, *Appl. Phys. Lett.*, 1997, **71**, 404.
4 L. Z. Meznar, B. Pracek, B. Orel and P. Bukovec, *Thin Solid Films*, 1998, **317**, 336.
5 C. Feldman and M. O'Hara, *J. Opt. Soc. Am.*, 1957, **47**, 300.
6 E. M. Rabinovich, J. Shmulovich, V. J. Fratello and N. J. Kopyov, *Am. Ceram. Soc. Bull.*, 1987, **6**, 1505.
7 J. Y. Choe, D. Ravichandran, S. M. Biomquist, D. C. Morton, K. W. Kirchner, M. H. Ervin and U. Lee, *Appl. Phys. Lett.*, 2001, **78**, 3800.
8 D. Ravichandran, R. Roy, A. G. Chakhovsoi, C. E. Hunt, W. B. White and S. Erdei, *J. Lumin.*, 1997, **71**, 291.
9 S. Chadha and J. J. Alwan, *US Pat.*, 1995, 5695809.
10 P. Rao, *Solid State Commun.*, 1996, **99**, 439.
11 A. Conde-Gallardo, M. Garcia-Rocha, I. Hemandez-Calderon and R. Palomino-Merino, *Appl. Phys. Lett.*, 2001, **78**, 3436.
12 J. Lin, D. U. Saenger, M. Mennig and K. Baerner, *Mater. Sci. Eng. B*, 1999, **64**, 73.
13 H. X. Zhang, C. H. Kam, Y. Zhou and X. Q. Han, *Thin Solid Films*, 2000, **370**, 50.
14 W. Tang and D. C. Cameron, *Thin Solid Films*, 1996, **280**, 221.
15 T. Minami, T. Miyata, T. Shirai and T. Nakatani, *Mater. Res. Soc. Symp. Proc.*, 2000, **621**, Q431.
16 J. Lin, M. L. Pang, Y. H. Han, Y. H. Zhou, M. Yu and H. J. Zhang, *Chin. J. Inorg. Chem.*, 2001, **17**, 153.
17 J. Lin and Q. Su, *Mater. Chem. Phys.*, 1994, **38**, 98.
18 J. Lin and Q. Su, *J. Mater. Chem.*, 1995, **5**, 1151.
19 M. J. J. Lammers and G. Blasse, *J. Electrochem. Soc.*, 1987, **134**, 2068.
20 J. Lin and Q. Su, *Phys. Status Solidi B*, 1996, **196**, 261.
21 T. J. Isaacs, *J. Electrochem. Soc.*, 1973, **120**, 654.
22 H. S. Kiliaan and G. Blasse, *J. Electrochem. Soc.*, 1989, **136**, 562.